View Article Online / Journal Homepage / Table of Contents for this issue

Ultra wide-field lens-free monitoring of cells on-chip†‡

Aydogan Ozcan§*[a] and Utkan Demirci§*[bc]

Received 6th September 2007, Accepted 2nd October 2007
First published as an Advance Article on the web 1st November 2007
DOI: 10.1039/b713695a

We experimentally and theoretically demonstrate the proof-of-principle of a new lens-free cell monitoring platform that involves using an opto-electronic sensor array to record the shadow image of cells onto the sensor plane. This technology can monitor/count cells over a field-of-view that is more than two orders of magnitude larger than that of a conventional light microscope. Furthermore, it does not require any mechanical scanning or optical elements, such as microscope objectives or lenses. We also show that this optical approach can conveniently be combined with microfluidic channels, enabling parallel on-chip monitoring of various different cell types, *e.g.*, blood cells, NIH-3T3 fibroblasts, murine embryonic stem cells, AML-12 hepatocytes. An important application of this approach could be a miniaturized point-of-care technology to obtain CD4 T lymphocyte counts of HIV infected patients in resource limited settings.

Published on 01 November 2007. Downloaded on 23/02/2016 01:37:49.

Introduction

There are more than 30 million HIV-infected people living in the developing world. The U.S. National Intelligence Council (NIC) predicts that this number would reach 80 million by 2010. Therefore, there is an urgent need for simple, low-cost and disposable diagnostic tools[1–8] that could be implemented in developing countries to increase access to HIV care and to improve treatment outcome.[3,4,7,9] On the other hand, such technologies face a significant, challenging task that requires monitoring or counting of hundreds to thousands of microscopic objects (*i.e.*, cells) simultaneously. Therefore, a simple, miniaturizable cell counting technology is needed, especially for global health related problems, such as HIV monitoring in resource limited settings. The objective of such a system is to develop a rapid, inexpensive, disposable and label-free CD4 T lymphocyte counting platform. A CD4 count less than 200 cells per microlitre of whole blood establishes the clinical diagnosis of AIDS. In most settings, antiretroviral therapy (ART) treatment is initiated at this critical value, since HIV-infected patients are then under risk for opportunistic infections.[10]

There are two significant problems that need to be addressed in order to count CD4 T lymphocytes from whole blood using a point-of-care technology: (1) capture/isolation of cells from whole blood in a high throughput manner, and (2) rapid counting of these captured/isolated cells. The first problem is addressed by fluorescent labeling or label-free microfluidic based techniques, as will be summarized below. The topic of this work, however, provides a new on-chip solution for the second problem of rapid counting of the captured/isolated cells.

There have been some recent studies addressing the above two issues of point-of-care cell counting.[1,4,5,11] For instance, a large scale fluidic approach was proposed, where all white blood cells are captured on a polycarbonate filter in a large scale device.[4] This initial cell isolation is not specifically selective towards CD4 T lymphocytes ($CD3^+$ $CD4^+$ cells). It captures all white blood cells on a porous filter. Therefore, an additional step, *i.e.*, a fluorescent labeling process, is utilized[4] to distinguish the CD4 T lymphocytes from other cells that are captured on the mechanical filter. The CD4 T lymphocytes are then counted under a fluorescence microscope using automated image recognition techniques. This method suffers from preprocessing and time consumption during fluorescent labeling of whole blood. Furthermore, the counting method requires capturing of images at multiple locations on a large mechanical filter using a fluorescent microscope. An average count using these multiple microscope images is given as the final count value. These issues make this fluorescent labeling based cell counting scheme less attractive for point-of-care applications.

Recently, label-free CD4 cell counting technologies have also been introduced.[2,5] These label-free approaches utilized microfluidic channels to capture cells by using surface chemistry with a high specificity and capture efficiency. However, in these label-free cell capturing techniques, counting is still performed under a regular microscope, and takes hours to quantify the capture on a single device. This creates a significant challenge to achieve a rapid point-of-care device. Although label-free capture/isolation of CD4 cells can be reliably achieved with the above discussed surface chemistry based microfluidic approaches,[2,5] rapid counting of the captured cells within a compact device volume still remains as a significant challenge, especially for point-of-care.

One proposed approach to solve this second problem is to use electrical spectroscopy[1] to quantify the captured/isolated cells in a microfluidic channel by monitoring changes in

[a]*Electrical Engineering Department, University of California, Los Angeles, CA, USA. E-mail: ozcan@ee.ucla.edu*
[b]*Bio-Acoustic-MEMS in Medicine (BAMM) Laboratory, Brigham and Women's Hospital, Harvard Medical School, Boston, MA, USA. E-mail: udemirci@rics.bwh.harvard.edu*
[c]*Harvard-MIT Health Sciences and Technology, Cambridge, MA, USA. E-mail: utkan@mit.edu*
† The HTML version of this article has been enhanced with colour images.
‡ Electronic supplementary information (ESI) available: Supplementary Figures S1–S3. See DOI: 10.1039/b713695a
§ The corresponding authors contributed equally to this work.

 This journal is © The Royal Society of Chemistry 2008

View Article Online

Published on 01 November 2007. Downloaded on 23/02/2016 01:37:49.

conductivity by captured cell lysis. However, it has issues to become a standard cell counting method due to the fact that captured cells of each patient may have varying ionic concentrations. This could lead to significant dynamic errors among patients as the number of captured cells increases. Furthermore, whole blood is a conducting ionic medium. Such an impedance based approach has to initially replace the whole blood in microfluidic channels with a non-ionic solution, keeping captured cells intact at place. Then, these cells have to be lysed and the resulting impedance change should be determined. Hence, such an impedance based system has to switch multiple solutions in the presence of captured cells in a microfluidic channel. Since the captured cells are degraded and are likely to lose ions as these various solutions are being replaced in a channel, this could also be a source of error for such a cell counting approach.

Therefore, we can conclude that the quantification/counting of captured/isolated cells within a microfluidic channel still remains as a major challenge that needs further attention for point-of-care HIV monitoring applications.[2,5] In this work, we aim to specifically address this problem, *i.e.*, we introduce a new on-chip cell counting platform that can be integrated with large area microfluidic channels to count hundreds of thousands of cells in seconds. Our proposed approach especially provides a quantification solution for specially prepared microfluidic channels[2,5] that can selectively capture *e.g.*, CD4 cells from whole blood at point-of-care. For this end, in this manuscript, we describe a lensless, ultra wide-field cell monitoring array platform based on shadow imaging (LUCAS), which relies on recording the shadow image of each individual cell (or a micro-scale particle) onto an opto-electronic sensor array plane. This lens-free optical approach increases the field-of-view of a conventional light microscope by at least two orders of magnitude and allows monitoring of hundreds of thousands of individual cells of various different cell populations in real time. Therefore, LUCAS can potentially monitor or count more than 100 times larger number of isolated cells with respect to a conventional light microscope, simultaneously within less than a few seconds, without expensive optical components, such as microscope objectives or lenses. Furthermore, LUCAS can also be integrated with microfluidic channels providing parallel on-chip monitoring and counting of cells. The simplified design also permits miniaturization of this technology that would make it especially suitable for resource limited settings.

There has been some recent progress on development of lensless on-chip imaging approaches.[12,13] However, quite different than LUCAS, these previous studies had rather small field-of-views (*e.g.*, less than 3.2 mm × 2.5 mm) and were not targeted towards on-chip cell monitoring or counting. They were designed to provide on-chip imaging of *e.g.*, *Caenorhabditis elegans*.[13] On the other hand, LUCAS does not aim to provide imaging of microscopic objects. It specifically targets the counting of captured cells or the monitoring in real time of the dynamic location of hundreds of thousands of individual cells on-chip over an ultra-wide field-of-view *e.g.*, a few centimetres by a few centimetres. Therefore, LUCAS does not aim to achieve a high spatial resolution, as long as cells within the field-of-view can yield enough contrast and signal-to-noise ratio on the sensor array to be monitored or counted individually. As will be illustrated in this work, LUCAS can provide these features with reduced complexity and ease of miniaturization.

The opto-electronic sensor array in LUCAS can be conveniently chosen to be a top-of-shelf 'charged-coupled device' (CCD) or a 'complementary metal-oxide semi-conductor' (CMOS) chip. For monitoring applications, where speed of image acquisition is important, CMOS based sensors will provide an advantage over CCD chips. However, for applications where image signal-to-noise ratio is more important (such as in automated cell counting/monitoring applications) CCD chips are preferred due to their better light sensitivity.

Fig. 1(a) shows a simplified sketch of a simple configuration of a LUCAS system to detect cells. Cells (in *e.g.*, a 1× phosphate buffer solution (PBS)) are placed between two microscope slides; and the sensor array plane lies right below the bottom microscope slide. In order to test the viability of this approach, the cells were tested under a regular high resolution microscope after they were placed between glass slides, and microscope images indicated no visible sign of cell deformation. In this configuration of Fig. 1(a), using a collimated optical beam, such as an incoherent white light source or a laser beam, the shadow of each cell falls onto the sensor array. However, our scheme does not use any optical components, such as lenses or microscope objectives, and purely relies on the fact that the distance between active regions of the sensor plane and location of cells is kept to less

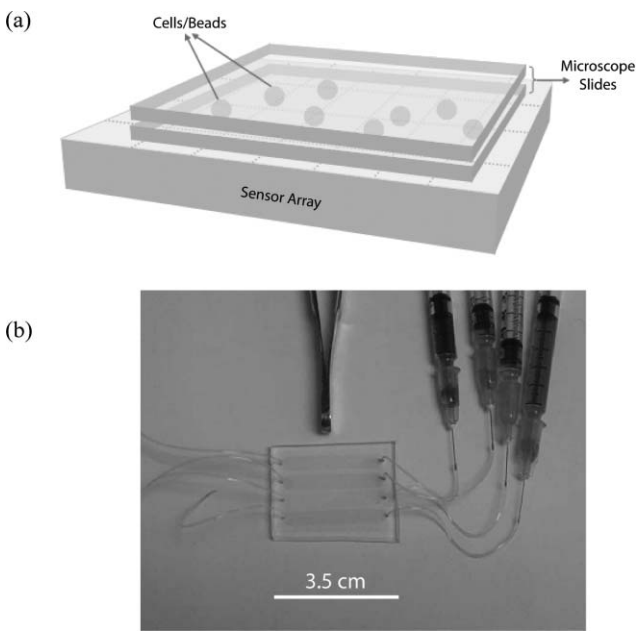

Fig. 1 (a) A simplified sketch of LUCAS. Cells to be imaged are illuminated by a collimated light source, and the shadow of each cell is recorded by an opto-electronic sensor array (*e.g.*, a CCD chip) without using any lenses. (b) A four channel microfluidic device that can be integrated with the LUCAS system. Such channels could be functionalized and used to selectively capture *e.g.*, CD4 cells from whole blood. LUCAS can monitor all 4 microfluidic channels simultaneously.

View Article Online

Published on 01 November 2007. Downloaded on 23/02/2016 01:37:49.

than ~200 μm to enable enough signal-to-noise ratio on the sensor plane. In the discussion to follow, further quantification of LUCAS performance as a function of the physical distance between the sensor and cell planes will be provided.

Another possible configuration for LUCAS utilizes a microfluidic device (fabricated *e.g.*, using polydimethylsiloxane (PDMS) based soft-lithography), where one or both sides of the microfluidic channel can be a thin glass microscope slide. One example of such a microfluidic device is shown in Fig. 1(b), where 4 independent, ~3 cm long, 50 μm high PDMS channels were fabricated on a 150 μm thin microscope glass slide, which can be used to locate cells within a microfluidic channel over an entire field-of-view of *e.g.*, 24 mm × 35 mm. Some LUCAS images of this microfluidic device will further be illustrated in the discussion to follow.

Theory behind LUCAS

For optimal operation of LUCAS, the distance between the active region of the sensor array (*e.g.*, active surface of the CCD chip) and the location of the imaged microscopic object (*e.g.*, cell population) is a critical parameter. To quantitatively investigate the effect of cell diameter on both the diameter of its shadow and on the detected signal strength, we numerically solved the Rayleigh–Sommerfeld diffraction integral[14] without making any paraxial approximations for various different physical distances (*i.e.*, z) between the detection and object planes. Since no lens is used in our detection system, we can model the operation principle of our system by numerically solving the Rayleigh–Sommerfeld diffraction equation. This numerical simulation assumed a coherent illumination at a wavelength (λ) of 633 nm and the refractive index of the microscope slide medium at this wavelength was taken as 1.45. The shadow diameter is estimated using full-width of the 10% of the maximum of the diffracted light intensity at the sensor plane. Finally, each cell is computationally modeled as a uniform circular object with a reduced field-transmission coefficient (*e.g.*, 0.5), whereas the surrounding fluid had a field transmission coefficient of 1.0. The results of this computation for z values of 50, 100, 150 and 200 μm are shown in Fig. 2(a–b).

Fig. 2(a) illustrates that for a given z value, there exists a certain cell diameter (D) that yields the smallest shadow diameter on the sensor plane, and this optimum cell diameter value shifts to larger values as z increases. This observation is related to a change (*i.e.*, a turning point) in the diffraction behavior of our optical system, and can be better understood by calculating the Fresnel number (N) of the system for each z and D values,[14] where $N = \pi D^2/(4z\lambda)$. For $N < 1$, our cell monitoring system is in the Fraunhofer region, where the shadow of cells on the sensor array will be a two-dimensional fractional Fourier transform of the initial cell distribution (located either in-between the microscope slides or within the microfluidic channel, Fig. 1). This explains the increasing shadow diameter for each z value as D reduces below a certain optimum value (*e.g.*, $D < 15$ μm for $z = 200$ μm), where $N = \pi D^2/(4z\lambda)$ quadratically reduces below 1, forcing the optical system further into the Fraunhofer region, which then causes significant spreading of shadow intensities.

Based on the same Rayleigh–Sommerfeld diffraction equation solutions given in Fig. 2(a), we can also estimate the relative change of the pixel strength on the sensor array as a function of both D and z. In this computation, for the sensor array, we assumed a 100% optical fill factor (*i.e.*, entire active area of the chip is used to detect photons) and a square pixel width of 10 μm. Results of Fig. 2(b) are computed for the central pixel of the sensor array (which is assumed to be right underneath a cell to be monitored, *i.e.*, stochastic nature of the cell distribution with respect to the pixel edges has been ignored for simplicity). Fig. 2(b) indicates that for all z values, signal strength of the central pixel of the sensor array increases almost linearly as a function of D, and after a certain D value is reached, it saturates. This behavior is consistent with Fig. 2(a) and can be qualitatively explained by the fact that in the Fresnel zone, increase in the shadow diameter is simply a result of a linear increase in D, rather than a diffraction related spreading effect.

Unlike a lens-based imaging system, choosing a smaller illumination wavelength does not always change cell shadow diameter. Fig. 2(c) shows the solution of the Rayleigh–Sommerfeld diffraction equation for a coherent illumination at various different wavelengths between 300 nm and 700 nm for a cell diameter of 20 μm. Under these conditions, LUCAS is in the Fresnel region for all wavelengths (300 nm–700 nm). For that reason, increasing the system spatial bandwidth by going to a smaller wavelength does not affect the shadow diameter, as shown in Fig. 2(c). However, for a smaller cell diameter *e.g.*, 5 μm and 2 μm as shown in Fig. 2(d–e), respectively, the system enters a phase between the Fraunhofer and Fresnel regions. In this case, using a smaller wavelength pushes the system closer to the Fresnel region than the Fraunhofer region, since $N \propto 1/\lambda$. This results in the diffraction induced spreading of the cell shadow to be reduced, which also shows itself in Fig. 2(d–e). To monitor/count different cell types, an important decision criteria for choosing the illumination wavelength is to check whether LUCAS is in the Fresnel region or not, by computing $N = \pi D^2/(4z\lambda)$, as indicated by Fig. 2(c–e). For a given experiment, where D and z values are fixed, an illumination wavelength that puts LUCAS into the Fresnel region should be chosen to reduce shadow diameter and hence increase contrast at the sensor plane. However, reducing λ even further, after the Fresnel region has been reached, provides no real benefit, as also illustrated in Fig. 2(c).

Experimental and results

After the basic theoretical understanding of LUCAS, we did some proof-of-principle experiments using polystyrene microbeads initially, and then using various cell types, such as NIH-3T3 fibroblasts, red blood cells, white blood cells and murine embryonic stem cells (mESC). For this purpose we used a CCD chip (KODAK, KAI-11002) that had over 11 million square pixels (9 μm wide), where the total active sensor array area was 37.25 mm × 25.70 mm. The protective glass coating on the CCD active area was removed so that the distance between the microscopic object of interest and the sensor plane could be better controlled. For our initial experiments, the large dimensions of the KODAK CCD chip

 This journal is © The Royal Society of Chemistry 2008

View Article Online

Published on 01 November 2007. Downloaded on 23/02/2016 01:37:49.

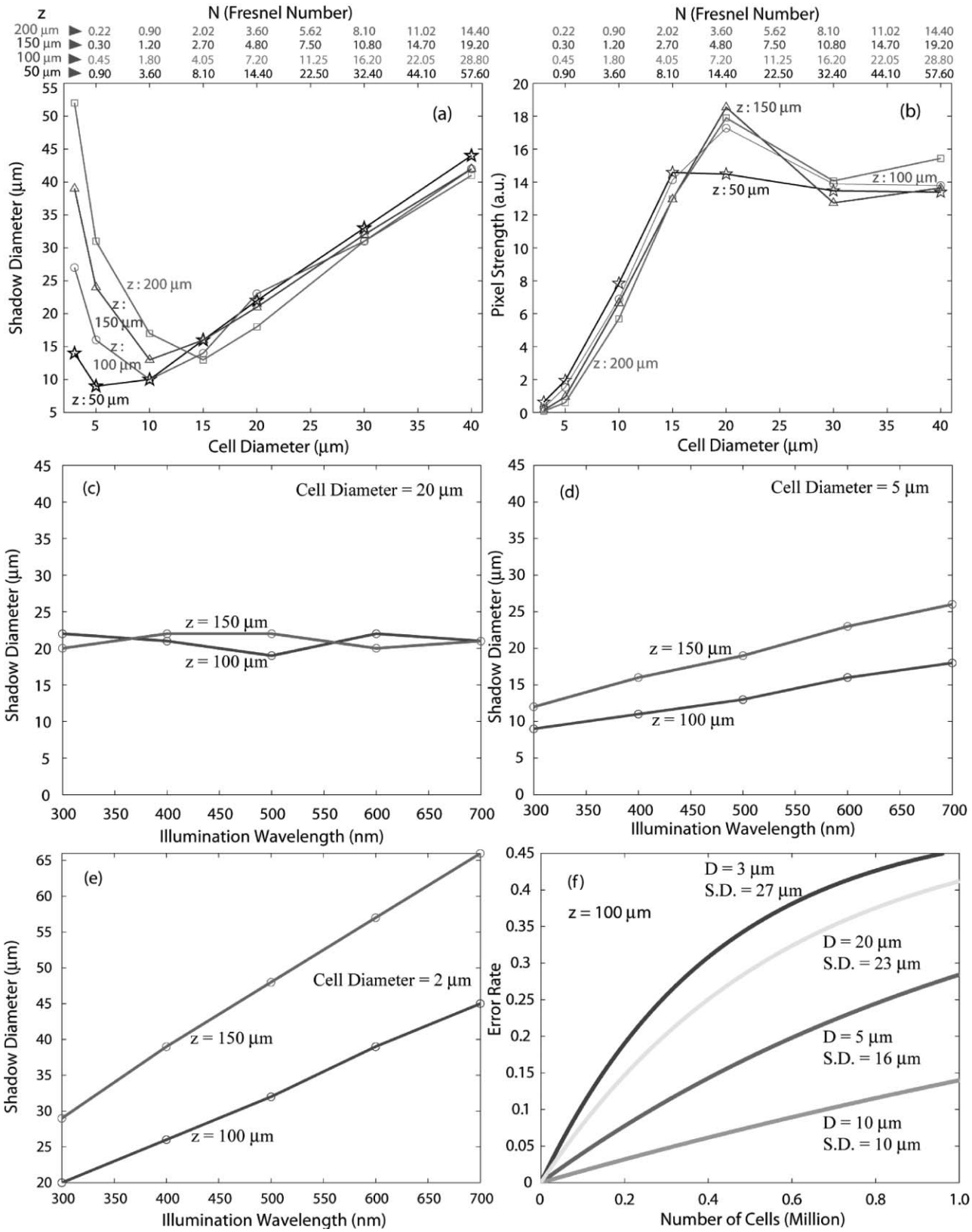

Fig. 2 (a) Shadow diameter of cells as a function of cell diameter. (b) Signal strength of cell shadow on the sensor array as a function of cell diameter. '*z*' refers to the physical distance between the active area of the sensor array and the cell population; (c–e) Shadow diameter of cells as a function of the illumination wavelength for cell diameter values of 20, 5 and 2 μm, respectively. (f) Error rate of on-chip cell counting as a function of the number of cells on the chip. "*D*" refers to the cell diameter and "*S.D.*" refers to the shadow diameter on the sensor array.

View Article Online

allowed us to use commercially available microscope slides with dimensions of 35 mm × 24 mm, with a thickness of 0.10–0.15 mm. In these initial experiments, we used two microscope slides facing each other, with microscopic objects placed in-between (see Fig. 1(a)). Later, we used multiple channel PDMS-glass microfluidic devices shown in Fig. 1(b).

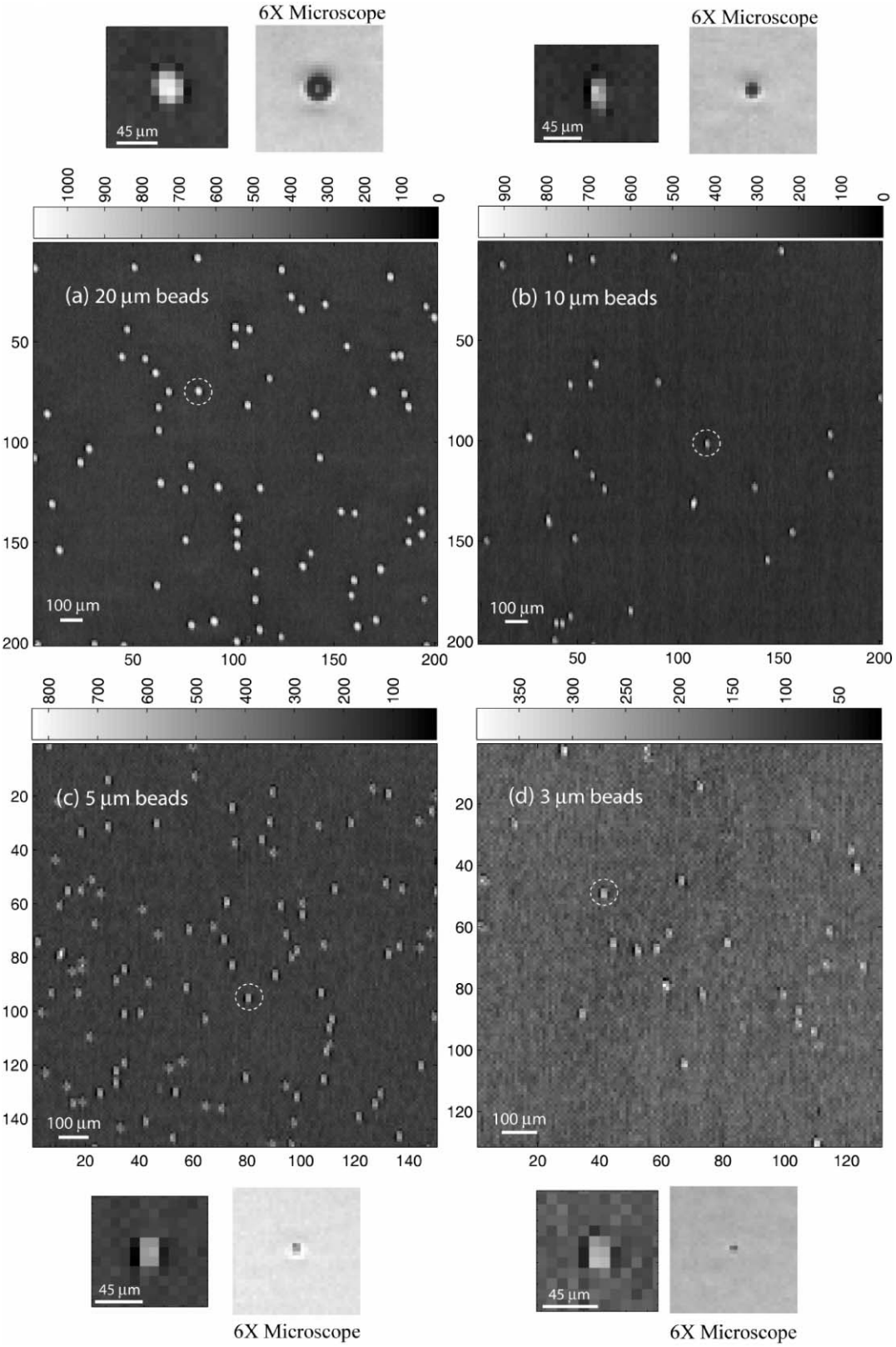

Fig. 3 LUCAS images of polystyrene microbeads of various different sizes. Each image has next to it, a zoomed version of a bead, and its comparison with a low NA microscope image.

Published on 01 November 2007. Downloaded on 23/02/2016 01:37:49.

 This journal is © The Royal Society of Chemistry 2008

View Article Online

Published on 01 November 2007. Downloaded on 23/02/2016 01:37:49.

The microscopic objects were injected into the microfluidic channels and monitored through the channel bottom.

Initially, to monitor microbeads of various sizes and concentrations, we diluted beads in deionized (DI) water. Fig. 3(a–d) show our initial results for 4 different sized polystyrene microbeads (Duke Scientific, CA, USA), with diameters of 20 $\pm$ 0.98 μm, 10 $\pm$ 0.73 μm, 5 $\pm$ 0.41 μm and 3 $\pm$ 0.15 μm, respectively. For these experiments, corresponding to Fig. 3(a–d), no lenses or microscope objectives were used. As shown in Fig. 1(a), CCD sensor plane simply recorded the shadow of each microbead after diffraction limited propagation of 0.15 mm through the bottom microscope slide. The illumination was achieved using an incoherent white light source, providing uniform illumination over the entire CCD area. Each frame in Fig. 3 also shows a zoomed version of a microbead (taken within a dotted circle) and its comparison with a microscope image taken using a 6× microscope objective. Here, we observe that LUCAS is not a full replacement for a wide-field microscope, since fine object features are lost due to diffraction and large pixel size. On the other hand, the target applications, such as point-of-care HIV monitoring in resource limited settings, do not require a high resolution microscope. The main objective of LUCAS is to enable a compact platform that can rapidly count cells over a large field-of-view or dynamically monitor the location of hundreds of thousands of cells simultaneously in real time.

It is evident from Fig. 3 that as the microbead diameter gets smaller, the recorded shadow image contrast gets weaker (see colorbars of Fig. 3). This is also in agreement with the conclusions of Fig. 2. However, even for 3 μm sized microbeads (see Fig. 3(d)), the available contrast in our shadow images is quite good for either the counting or monitoring purposes described above. To illustrate this fact, Fig. 4(a–b) show the detection of microscopic object locations using a commercially available computer program for 3 μm and 5 μm diameter beads, respectively. The program uses custom image recognition algorithms based on matched filtering, binary image processing, moment calculations and pattern classification to identify each object. Adaptive techniques were used to account for variations in background and object image brightness variations across the entire field-of-view. The results presented in Fig. 4 demonstrate the potential for computer-assisted automated detection, monitoring and/or counting of microscopic objects using LUCAS. Fig. 4(a) shows 22 microbeads of 3 μm diameter in a $\sim$2 mm^2 area and Fig. 4(b) shows 70 beads of 5 μm diameter in also a $\sim$2 mm^2 area. This operation can easily be extended to the entire image area to give the total number of microbeads within a field-of-view of 37.25 mm × 25.70 mm.

To further investigate the effect of a reduction in the microbead diameter, we also imaged 1 μm diameter beads (see supplementary Fig. S1(a)‡). By using only a pixel size of 9 μm at the CCD sensor chip, we can still identify the shadow of individual 1 μm sized particles. Further, using digital filtering, such as two-dimensional (2D) adaptive Wiener filtering,[15] we can digitally improve the contrast and signal-to-noise ratio of the presented shadow images. The adaptive 2D Wiener filter is widely used in other imaging applications,[16] such as optical coherence tomography or ultrasound, and simply computes

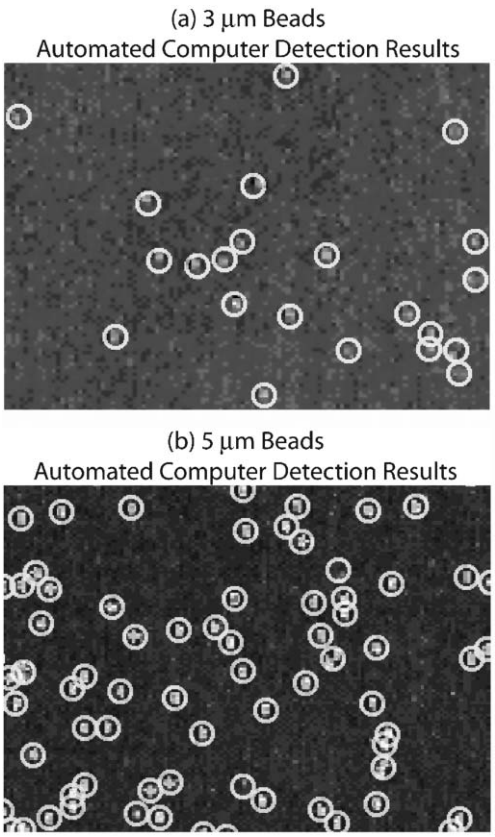

Fig. 4 Computer assisted automated detection of the dynamic location of microparticles. (a) 22 microbeads of 3 μm diameter in a $\sim$2 mm^2 area are counted. (b) 70 beads of 5 μm diameter in a $\sim$2 mm^2 area are counted.

local mean and variance inside a window centered on each pixel of the input image. These local statistics are then used adaptively to generate a pixelwise Wiener filter. The entire image is filtered by repeating the same procedure for each pixel. The improved results of the 2D Wiener filter especially shows itself for 1 μm sized beads: the signal-to-noise ratio (SNR) and contrast-to-noise ratio (CNR) of the filtered image (see supplementary Fig. S1(b)‡) is improved by $\sim$5 dB and $\sim$2 dB, respectively, where SNR and CNR are defined as:[16] $\mathrm{SNR} = 10\log_{10}(\max\{I^2\}/\sigma_b^2)$ and $\mathrm{CNR} = (1/R)\sum_{r=1}^{R}(\mu_r - \mu_b)\Big/\sqrt{\sigma_r^2 + \sigma_b^2}$, respectively, where I is the linear magnitude image, μ_b and σ_b^2 are the mean and variance of I in a background noise region, and finally μ_r and σ_r^2 are the mean and variance of all regions of interests (R). In our numerical computation for the supplementary Fig. S1,‡ we used R = 3, excluding the background region. Such powerful digital filters[16] can be quite useful, especially for computer based automated counting and monitoring (*e.g.* tracking) of cells by providing improvement in acquired image SNR.

Next, we performed experiments with LUCAS using various cell types, *i.e.*, monocytes, NIH-3T3 fibroblasts, mESCs and red blood cells. Fig. 5(a–c) shows shadow images for some of these cell populations. For these experiments, an incoherent white light source is used to provide uniform illumination over the entire CCD sensor area, *i.e.*, 37.25 mm × 25.70 mm. Cells

View Article Online

Published on 01 November 2007. Downloaded on 23/02/2016 01:37:49.

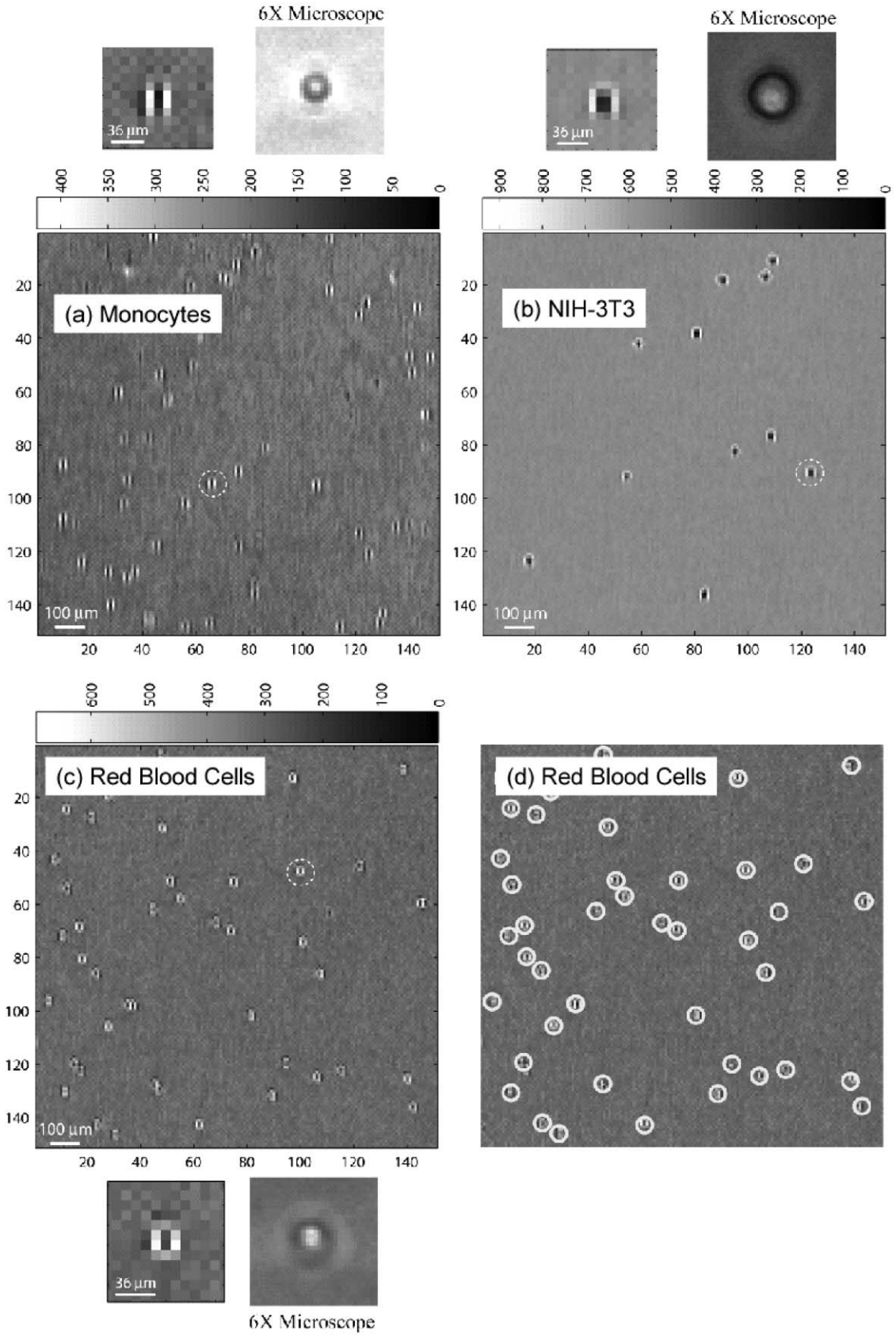

Fig. 5 LUCAS images for (a) monocytes, (b) NIH-3T3 fibroblasts, (c) red blood cells. Each image has next to it, a zoomed version of a cell, and its comparison with a low NA microscope image. (d) Computer assisted automated detection of the dynamic location of the red blood cells. A total of 41 cells are counted within a field of view of 1.4 mm × 1.4 mm.

 This journal is © The Royal Society of Chemistry 2008

View Article Online

Published on 01 November 2007. Downloaded on 23/02/2016 01:37:49.

to be imaged were gently placed between two microscope slides in PBS, as illustrated in Fig. 1(a). The contrast in these cell images (Fig. 5(a–c)) is high enough for cell counting/monitoring purposes, proving the usefulness of the proposed technology. To illustrate this point, Fig. 5(d) shows the results of the same commercial computer software (see Fig. 4) for detection of the location of each individual red blood cell of Fig. 5(c). A total of 41 cells were counted within a field of view of 1.4 mm × 1.4 mm. This operation can easily be performed across the full image area giving the total number of cells within a field-of-view of 37.25 mm × 25.70 mm.

To further illustrate the performance of LUCAS, Fig. 6(a), (see as well supplementary Fig. S2(a) and S3(a)‡) show the full-frame images of the CCD chip for red blood cells, NIH-3T3 fibroblasts and mESCs, respectively, where the full field-of-view is 37.25 mm × 25.70 mm, *i.e.* entire area of the CCD chip. **Note that in these figures the scale bar is "*1 cm*".** When compared to the field-of-view of a conventional light microscope using 5× or 10× microscope objectives, LUCAS presents two orders of magnitude wider field-of-view (in Fig. 6(a), supplementary Fig. S2(a)‡ and supplementary Fig. S3(a)‡, typical field-of-view of 5× and 10× microscope objectives are shown with dashed curves). Fig. 6(b–i), (see also supplementary Fig. S2(b–i), Fig. S3(b–e)‡) demonstrate zoomed images of various locations on a LUCAS image for red blood cells, NIH-3T3 fibroblasts and mESCs, respectively. According to these figures, using LUCAS, we can monitor/count individual cells over a field-of-view as large as 37.25 mm × 25.70 mm simultaneously, without using optical lenses or microscope objectives. Furthermore, using a commercially available larger area CCD or CMOS sensor, the field-of-view demonstrated in this paper can be improved.

In order to estimate the error rate in LUCAS to count cells, we developed an approximate model to calculate the cell overlap probability to predict the maximum number of cells that can be detected on an opto-electronic sensor area. Let us assume that $A_{\text{cell\_shadow}}$ is the area of a single cell shadow on the sensor plane, and A_{sensor} is the active area of the sensor, then $N_0 = A_{\text{sensor}}/A_{\text{cell\_shadow}}$ will give the sensor to object area ratio. If there are N cells to be imaged, then the fraction of cell shadows that do not overlap can be given by $F(N) = e^{-4(N/N_0)}$

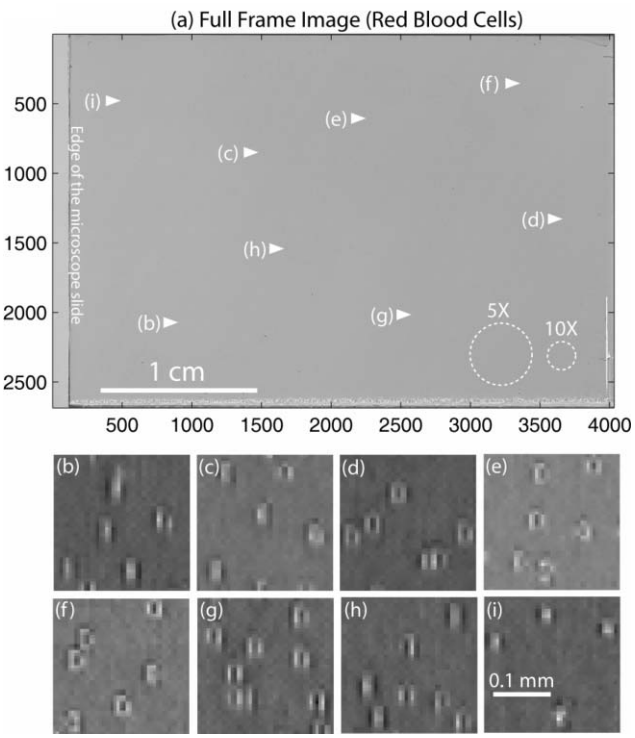

Fig. 6 (a) LUCAS full-frame image for red blood cells. The field-of-view of this frame is ~37 mm × 26 mm. (b–i) Zoomed images of different regions of Fig. 6(a).

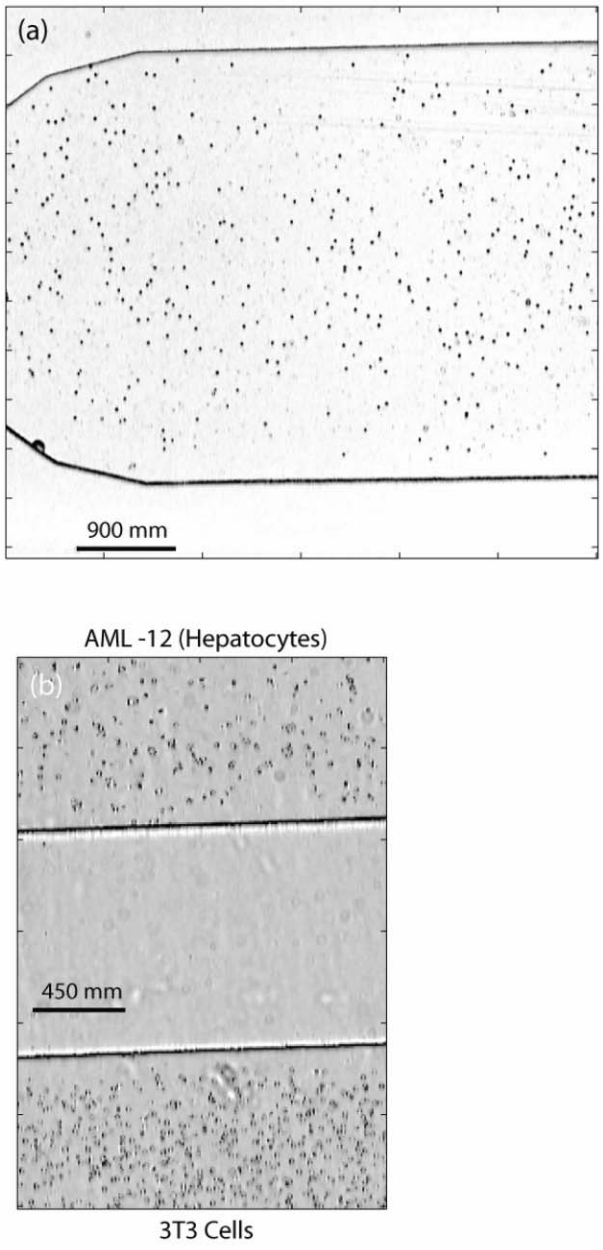

Fig. 7 (a) 20 μm diameter polystyrene microbeads imaged within a microfluidic chip without using lenses. (b) Hepatocytes and fibroblasts are imaged within two different microfluidic channels using the same LUCAS configuration.

View Article Online

Published on 01 November 2007. Downloaded on 23/02/2016 01:37:49.

for $N \gg N_o$.[17] The number of non-overlapping cell shadows is then given by $N_{\text{non-overlapping}} = Ne^{-4(N/N_0)}$. Therefore, to a first order approximation, the error rate in the count result of LUCAS can be estimated as, error rate = $(1 - e^{-4(N/N_0)})/2$. Using this model, for 3 μm, 5 μm, 10 μm, and 20 μm cell diameter values, and for a microscope slide thickness of $z = 100$ μm, we can calculate the error rate for count results of LUCAS as a function of the number of cells, Fig. 2(f). The results indicate that to guarantee an error rate of less than 10%, the maximum number of 3 μm, 5 μm, 10 μm, and 20 μm diameter cells that can be counted using LUCAS should be 0.93×10^5, 2.66×10^5, 6.80×10^5 and 1.29×10^5, respectively. Note that since the shadow width for these cell diameter values is important for LUCAS (see Fig. 2(a)), the highest number of cells that can be counted using LUCAS using the described configuration is the 10 μm cell line, with a maximum cell number of 0.68 million cells. A larger area sensor chip would increase these values.

Finally, we investigated the performance of LUCAS to monitor microbeads and cells in PDMS–glass based microfluidic channels. One example of such a microfluidic channel was shown in Fig. 1(b), where 4 independent, ~3 cm long, 50 μm high PDMS channels were fabricated on a 150 μm thin microscope glass slide. Using such microfluidic devices, we achieved similar contrast and signal-to-noise ratios to monitor microbeads and cells within these channels. Fig. 7 illustrates our initial results, where 20 μm diameter microbeads and two different cell lines (fibroblasts and hepatocytes) were simultaneously monitored in microfluidic channels on a single chip using LUCAS. These results demonstrate the potential of the proposed lens-free optical approach to monitor/count various types of captured cells within a microfluidic device,[2,5] providing a potential solution to a significant problem in point-of-care cell counting technologies. In our future work, this technology will be integrated with surface chemistry based microfluidic devices to selectively capture and count CD4 and other cell types from whole blood using clinical samples taken from HIV patients. The operation principles and the potential strength of LUCAS have been demonstrated in this manuscript towards such microfluidic based HIV monitoring applications.

Conclusions

In conclusion, we have experimentally demonstrated the proof-of-principle of a new, lensless, ultra wide-field cell monitoring array platform based on shadow imaging (LUCAS). LUCAS can potentially enable real-time monitoring or counting of live cells, simultaneously, over a field-of-view that is more than two orders of magnitude larger than that of conventional light microscopy. LUCAS does not require mechanical scanning or additional optical elements, such as microscope objectives or lenses. Furthermore, LUCAS can be integrated with microfluidic devices to allow parallel monitoring and counting of various different cell types (*e.g.*, blood cells, fibroblasts, embryonic stem cells, hepatocytes) in a controlled manner on-chip. Some important applications of LUCAS would include providing a rapid cell counting diagnostic tool for CD4 HIV monitoring in resource limited settings; or real-time on-chip monitoring of motility, growth and function of cell populations over extended periods of time using a large field-of-view of a few centimetres by a few centimetres.

References

1 X. Cheng, Y. Liu, D. Irimia, U. Demirci, L. Yang, L. Zamir, W. Rodriguez, M. Toner and R. Bashir, *Lab Chip*, 2007, **7**, 746–755.
2 X. Cheng, D. Irimia, M. Dixon, J. C. Ziperstein, U. Demirci, L. Zamir, R. G. Tompkins, M. Toner and W. R. Rodriguez, *JAIDS, J. Acquired Immune Defic. Syndr.*, 2007.
3 M. J. Butte, A. P. Wong, A. H. Sharpe and G. M. Whitesides, *Clin. Immun.*, 2005, **116**, 282.
4 W. R. Rodriguez, N. Christodoulides, P. N. Floriano, S. Graham, S. Mohanty, M. Dixon, M. Hsiang, T. Peter, S. Zavahir, I. Thior, D. Romanovicz, B. Bernard, A. P. Goodey, B. D. Walker and J. T. McDevitt, *PLoS Med.*, 2005, **2**, e182.
5 X. Cheng, D. Irimia, M. Dixon, K. Sekine, U. Demirci, L. Zamir, R. G. Tompkins, W. Rodriguez and M. Toner, *Lab Chip*, 2007, **7**, 170–178.
6 P. Balakrishnan, M. Dunne, N. Kumarasamy, S. Crowe, G. Subbulakshmi, A. K. Ganesh, A. J. Cecelia, P. Roth, K. H. Mayer, S. P. Thyagarajan and S. Solomon, *JAIDS, J. Acquired Immune Defic. Syndr.*, 2004, **36**, 1006–1010.
7 V. Linder, S. K. Sia and G. M. Whitesides, *Anal. Chem.*, 2005, **77**, 64–71.
8 J. Cohen, *Science*, 2004, **304**, 504–509.
9 J. Cohen, *Science*, 2004, **304**, 1936.
10 Patient Monitoring Guidelines for HIV Care and ART, World Health Organization, 2005, available at http://www.who.int/hiv/pub/guidelines/patientmonitoring.pdf.
11 C. D. Chin, V. Linder and S. K. Sia, *Lab Chip*, 2007, **7**, 41–57.
12 X. Heng, D. Erickson, L. R. Baugh, Z. Yaqoob, P. W. Sternberg, D. Psaltis and C. Yang, *Lab Chip*, 2006, 1274–1276.
13 D. Lange, C. W. Storment, C. A. Conley and G. T. A. Kovacs, *Sens. Actuators, B*, 2005, **107**, 904–914.
14 M. Gu, *Advanced Optical Imaging Theory*, Springer-Verlag, Berlin, 1999.
15 S. J. Lim, *Two-Dimensional Signal and Image Processing*, Prentice Hall, Englewood Cliffs, NJ, 1990.
16 A. Ozcan, A. Bilenca, A. E. Desjardin, B. E. Bouma and G. J. Tearney, *J. Opt. Soc. Am. A*, 2007, **24**, 1901.
17 P. Sethu, M. Anahtar, L. L. Moldawer, R. G. Tompkins and M. Toner, *Anal. Chem.*, 2004, **76**, 6247–6253.

 This journal is © The Royal Society of Chemistry 2008